

Supplement of Atmos. Chem. Phys., 19, 245–258, 2019
<https://doi.org/10.5194/acp-19-245-2019-supplement>
© Author(s) 2019. This work is distributed under
the Creative Commons Attribution 4.0 License.



Supplement of

An overview of airborne measurement in Nepal – Part 1: Vertical profile of aerosol size, number, spectral absorption, and meteorology

Ashish Singh et al.

Correspondence to: Ashish Singh (ashish.singh@iass-potsdam.de)
and Maheswar Rupakheti (maheswar.rupakheti@iass-potsdam.de)

The copyright of individual parts of the supplement might differ from the CC BY 4.0 License.

Supplementary

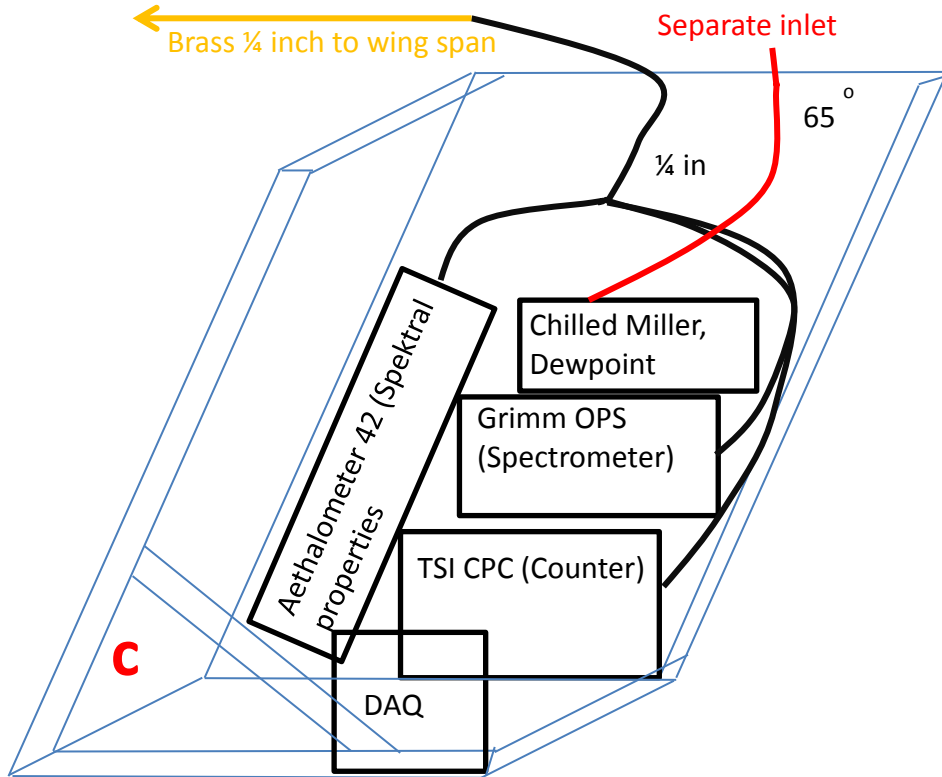
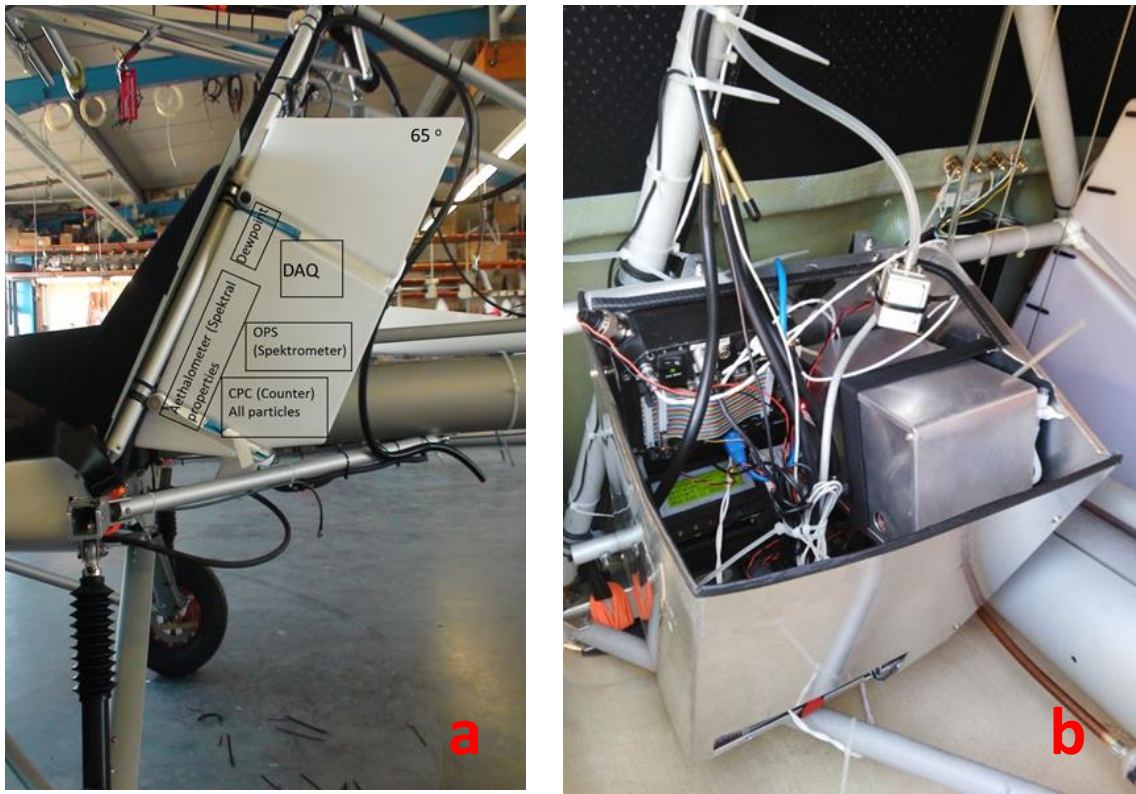


Figure S1: Testing and assembly of the instrument package inside IKARUS-C42 in the COMCO IKARUS station in Germany (a) field station in Pokhara Valley (b) sketch of the Instrument package (c)

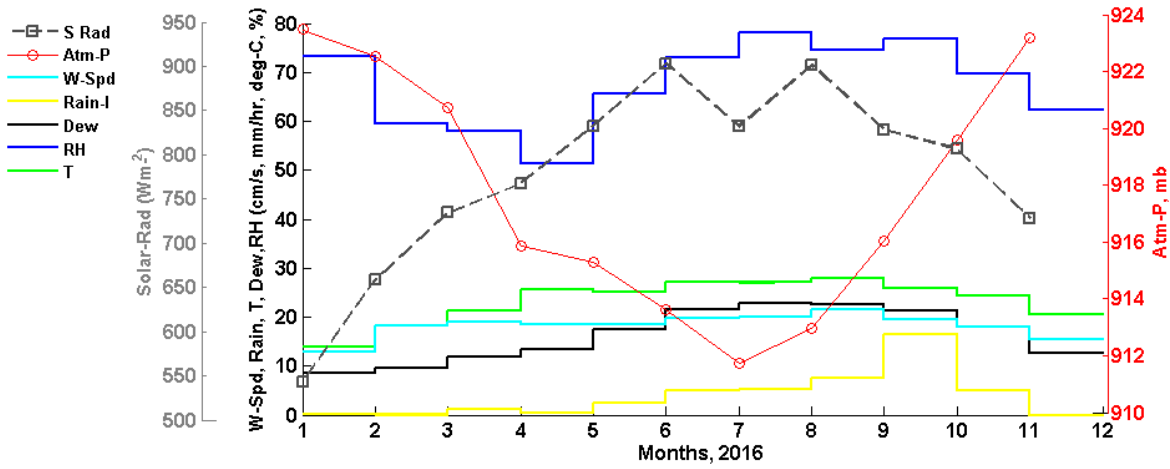


Figure S2: Monthly mean values of key meteorological parameters measured at the Pokhara regional airport (*station ID: 804, 28.1993528, 83.9784028, 820 meters altitude*) using an *ENVIRODATA weather station*. December 2016 is missing due to data availability. The monthly value of solar radiation shown here is 95 percentile of the daily values to reflect the peak insolation values. Wind speed and rainfall intensity are 10x for graphical clarity. Note that rainfall values presented here are not cumulative over a month, rather average of the month. (December data is not available)

The annual mean temperature in the valley was 22° C, with the lowest monthly mean in January (~15° C) and the highest in July (~ 25° C). Rainfall was also highest in the months of August and September (summer monsoon season), followed by relatively dry post-monsoon (October-November) and winter period (December-February). The late pre-monsoon to summer monsoon were also the periods of maximum monthly solar insolation (~900 Wm⁻²) and the insolation is approximately half (~550 Wm⁻²) during the winter

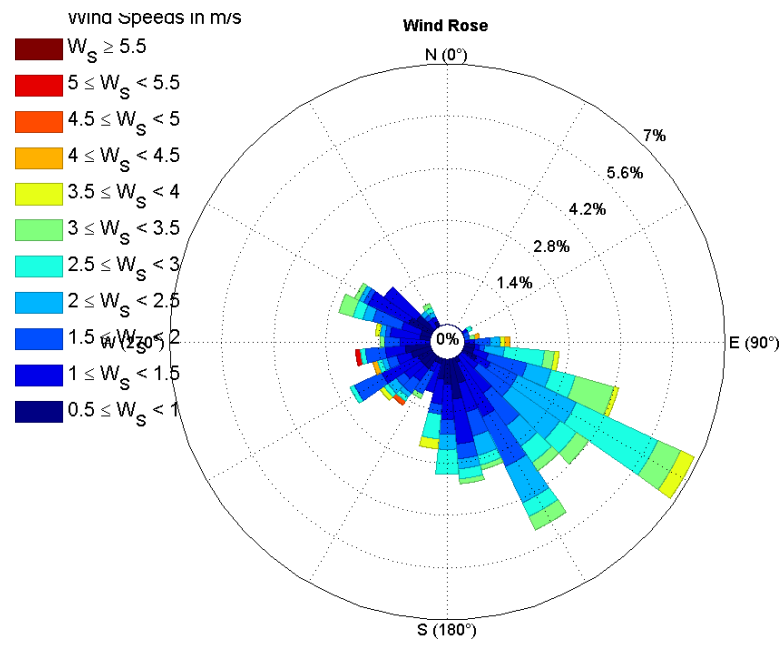


Figure S3: Frequency of wind speed and direction observed in the Pokhara Valley during May 2016

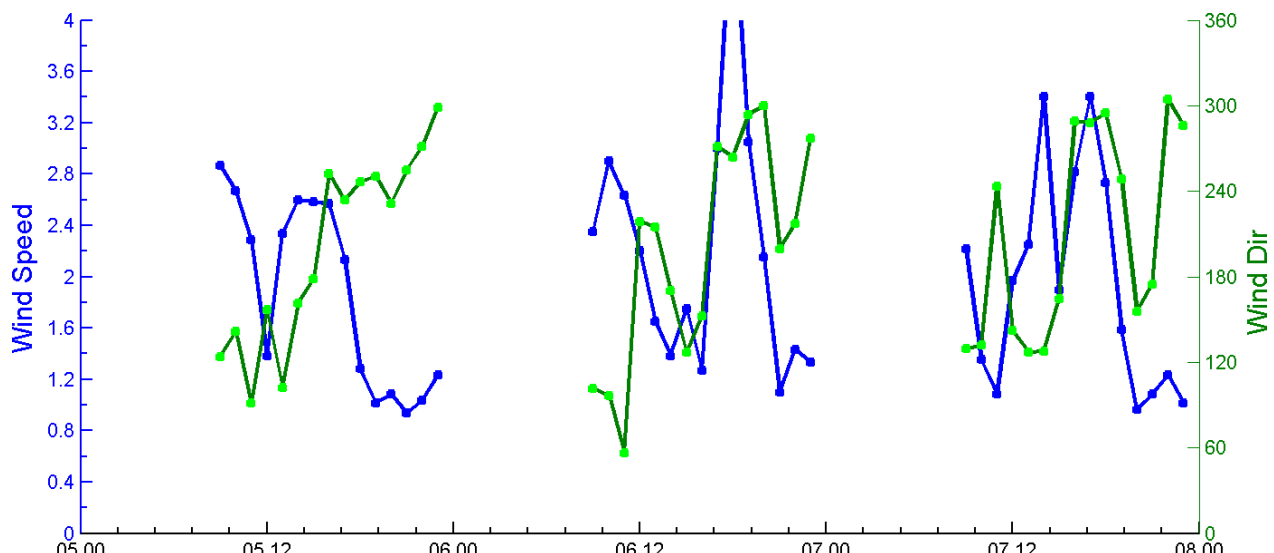


Figure S3.1: Wind speed (ms^{-1}) and direction from 5-7 May 2016 measured at the Pokhara Regional Airport meteorological station

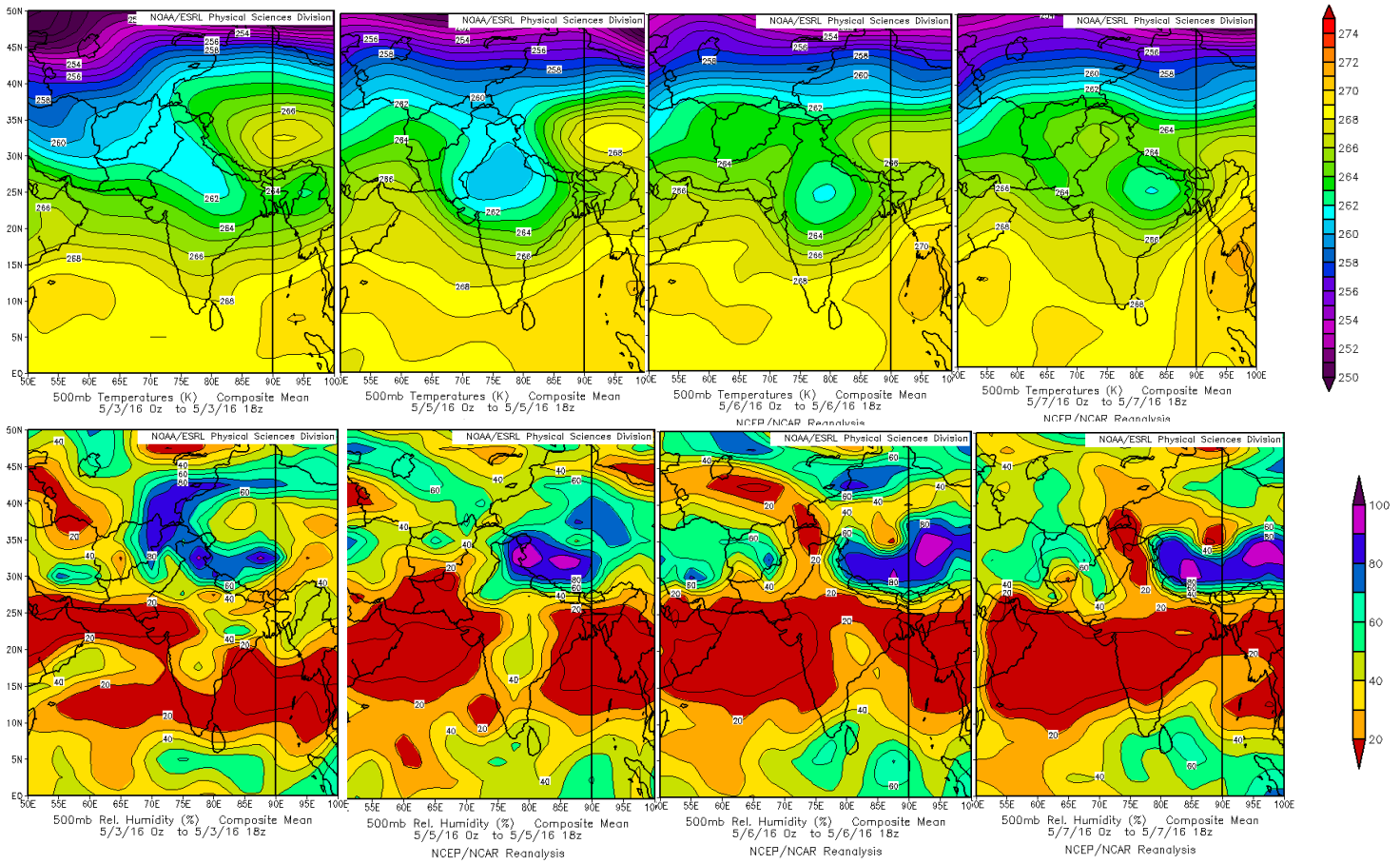


Figure S4: Daily temperature and relative humidity at 500mb using the NCEP NCAR reanalysis ($2.5 \times 2.5^{\circ}$) data over South Asia from May 1 to 7 2016.

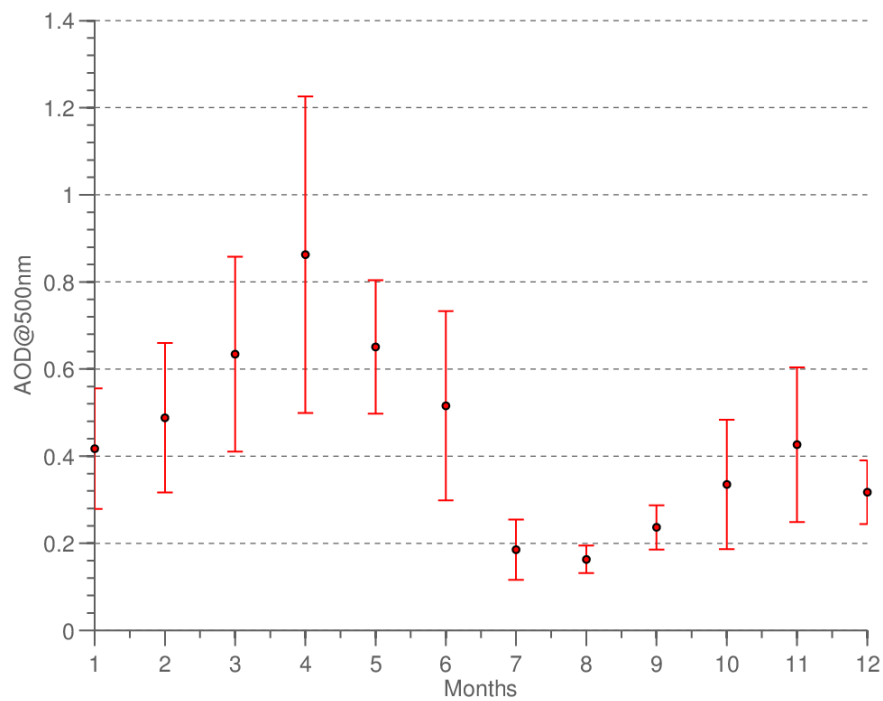


Figure S5: Monthly mean value of AOD 500 nm in Pokhara Valley for 2010-2016 (Note: Level 2 and 1.5 were used)

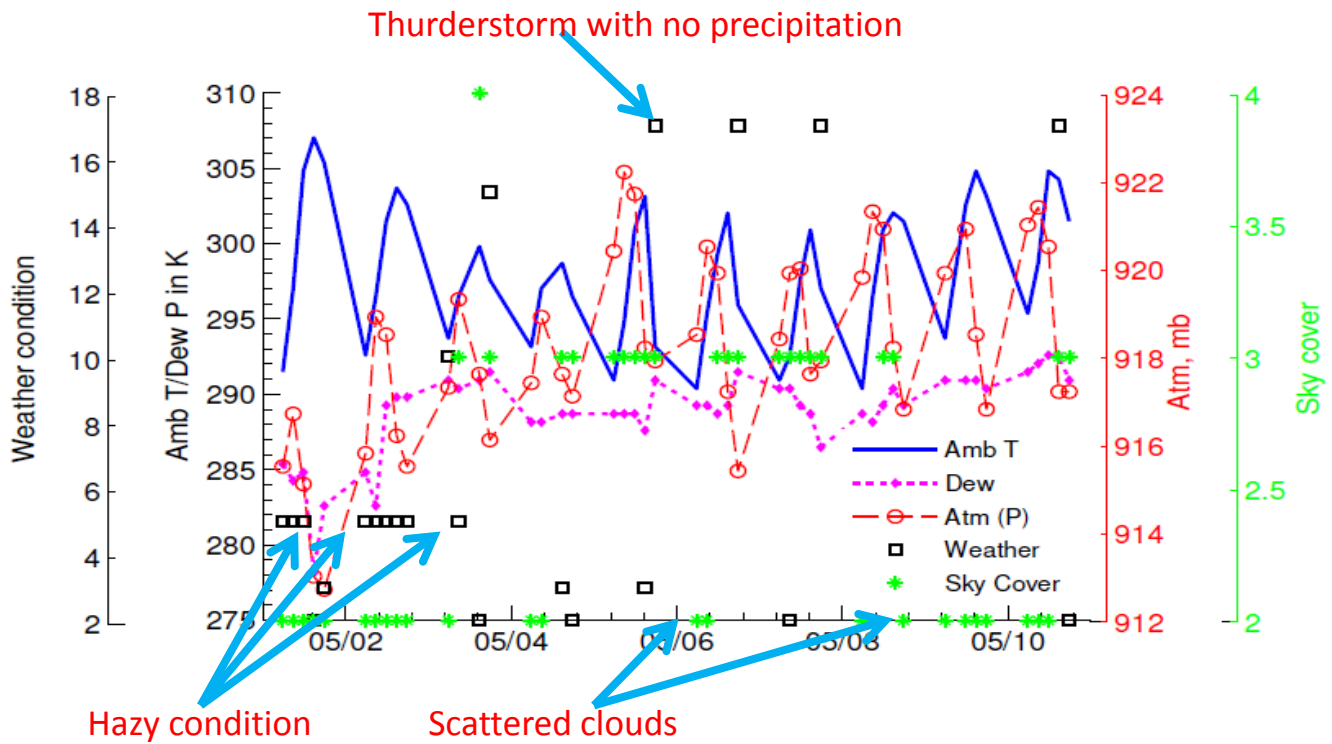


Figure S6: Local Meteorology in the Pokhara Valley from 1-10 May 2016.

Weather condition is coded by individual number (see NOAA <https://www7.ncdc.noaa.gov/CDO/dataproduct> for details). Weather condition in the figure is shown as a black square box. Weather condition of 5 indicate Hazy conditions; 17-thunderstorm but no precipitation; 3-cloud generally forming; 2-sky unchanged

The sky cover is numerically coded as follows:

CLEAR =1, SCATTERED (1/8 TO 4/8) =2, BROKEN-5/8 TO 7/8 =3, OVERCAST=4, OBSCURED=5, PARTIAL OBSCURATION=6

(Also see NOAA <https://www7.ncdc.noaa.gov/CDO/dataproduct> for details).

S7: Summary of aerosol properties using AERONET measurement from 2010-2016

AERONET measurements (Holben et al., 1998) have been made in the Pokhara Valley since January 2010. The AERONET station (83.97° N, 28.18° E, 807 m a.s.l.) is approximately 1.1 km southeast from the Pokhara Regional Airport, located in the semi-urban area of Pokhara City. Cloud-screened and quality assured (level 2) data were used in the study. Gaps in the level 2 data were supplemented with level 1.5 data. The AERONET retrieval suffers in the monsoon months (June to September) due to interference by monsoon clouds in the Pokhara Valley, as indicated by the gap in Figure 2.

A combination of direct products such as aerosol optical depth (AOD) and inversion products such as fine AOD, absorption Ångstrom exponent (AAE) and volume size distribution were used for the analysis presented in this study. The typical reported uncertainty in the AERONET data products for AOD (> 0.04) is approximately ± 0.01 to ± 0.02 , and is higher for shorter wavelengths (Eck et al., 1999; Holben et al., 1998). The observed uncertainty in AOD also influences other AERONET products such as the Ångstrom exponent (AE) and the inversion products. Thus these derived products will have a higher uncertainty than the AOD (Schuster et al., 2006; Dubovik and King, 2000). Further details about the AERONET direct and inverted data products can be found in Holben et al. (2006).

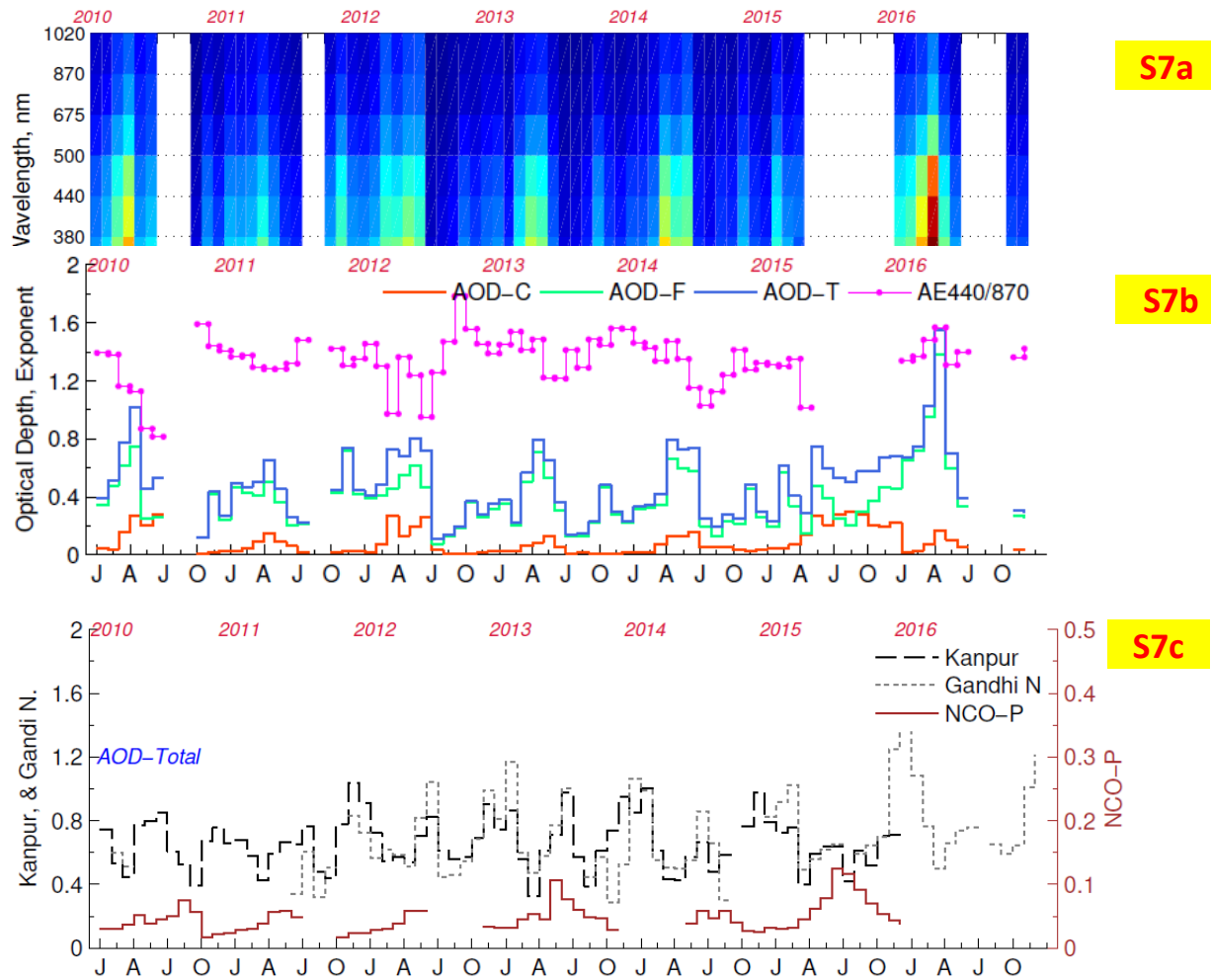
In the Pokhara Valley, AOD values showed a strong seasonality in the wavelength bands between 340 and 1020 nm. The inter-annual variation in the AOD during 2010-2016 was closely associated with the enhancement in the fine-mode fraction, and to a lesser extent in the coarse mode for dust (Xu et al., 2014). The observed inter-annual variation in the AOD could be influenced by the interaction between aerosols and the mesoscale to synoptic-scale meteorology (Vinoj et al., 2014; Ram et al., 2010; Kaskaoutis et al., 2012a), as well as influences of the ENSO (El Niño southern oscillation) on West Asia and the IGP (Kim et al., 2016). AOD values were enhanced or elevated during the winter, with the aerosol load building up throughout the pre-monsoon months ($AOD_{500nm} > 0.6$, Figure 3a, 3b, and S5) and then falling to their lowest values in the monsoon months ($AOD_{500nm} \sim 0.2\text{-}0.3$), most likely due to wet removal of aerosols. After the low AOD during the monsoon, AOD gradually increases (to $\sim 0.4\text{-}0.5$) during the post-monsoon through winter to the pre-monsoon season. AOD was usually highest in April ($AOD_{500nm}: 0.86 \pm 0.36$), followed by March, May, and June. The increase in aerosols load (as reflected by the AOD) during the pre-monsoon months can also be seen at high altitude sites such as the NCO-P site in the Khumbu Valley near Mt. Everest, located at 5057 m (a.s.l.) and about 300 km to the east of Pokhara (see Figure 3c), as well as at IGP sites in Kanpur (130 m a.s.l., 400 km southwest of the Pokhara Valley) and Gandi Nagar (60 m a.s.l., 250 km south of the Pokhara Valley). A similar AOD build-up was

also observed by Ram et al. (2010) in Darjeeling (2194 m a.s.l., hill station ~450 km east of Pokhara Valley), and by Chatterjee et al. (2012) in Manora Peak (1950 m a.s.l., 460 km west of Pokhara Valley). This regional increase in aerosol load in the IGP and the Himalayan region is partly due to active transport during the pre-monsoon season, often linked with westerly advection bringing dust from West Asia and nearby arid regions (Gautam et al., 2011). The relatively dryness with little precipitation during this period also contributes to the total aerosol load, since washout will be limited. The AOD peaks occur in different months in these different sites in the IGP and Himalayas, reflecting the varying influence of local meteorology and increase in the emission sources such as agriculture residue burning dominated by dominated by fine-mode particles (Putero et al., 2014).

Fine-mode aerosol particles scatter more at shorter wavelengths (such as 340-500 nm) compared to 1020 nm (Schuster et al., 2006). The variation in the Ångstrom exponent was not as definitive as in the AOD values; the Ångstrom exponent was generally below 1 during pre-monsoon months and above 1 in the post-monsoon and winter months. Ångstrom exponent values of >1 are generally reported for sources such as biomass burning, fossil fuel combustion and other primary sources which have a dominant fine-mode fraction. Dust and other coarse-mode aerosols have Ångstrom exponents less than 1 (Eck et al., 1999). The highest values of the Ångstrom exponent (at least >1.2) were observed for the post-monsoon observation period, presumably due to emissions of primary fine-mode aerosol from sources such as open burning of agriculture, often reported in this season especially to the south and southeast of Pokhara Valley and in the IGP. In addition to the Ångstrom exponent, the temporal variation of AOD fine and coarse modes (at 500 nm) in Figure 3b and 3c also indicates that fine-mode aerosols nearly exclusively dominate the atmospheric column during the post-monsoon and winter seasons. In the pre-monsoon season, in addition to the fine-mode, a substantial fraction of coarse-mode also exists, which is also observed in the monsoon season.

On the nature of aerosols or bulk composition, Figure 3e shows a simple scatter-plot based on the absorption and extinction Ångstrom exponents (AAE and EAE at 440-870 nm) which can be used to indicate the aerosol types (Giles et al., 2011; Giles et al., 2012; Dubovik et al., 2002). These two parameters describe the spectral dependence or “slope” of aerosols absorption and extinction at the measured wavelength (Seinfeld and Pandis, 2006). Extinction exponent is a proxy for aerosol size, while the absorption exponent is a proxy for absorbing aerosols including a mixed aerosol. The classification employed by Giles et al. (2011) based on observations from the IGP AERONET sites defines “*Dust*” or “*Mostly Dust*” aerosols within the range of EAE <0.5 and AAE >2.0 and “*Mostly BC like*” aerosols with EAE <0.8 and AAE ~1.0-2.0. Urban/industrial and biomass burning aerosols fall under the “*Mostly*

BC" category (Dubovik et al., 2002; Giles et al., 2011). The mixed aerosol ("Dust+BC") centers around a value of EAE \sim 0.5 and AAE \sim 1.5. Based on this approximate classification from a monthly data, the dominant aerosol in the Pokhara Valley is mostly *BC like*; however, the daily aerosol characteristics can vary from more mixed to dust-like in the pre-monsoon months, to more BC-like in the post-monsoon and winter months.



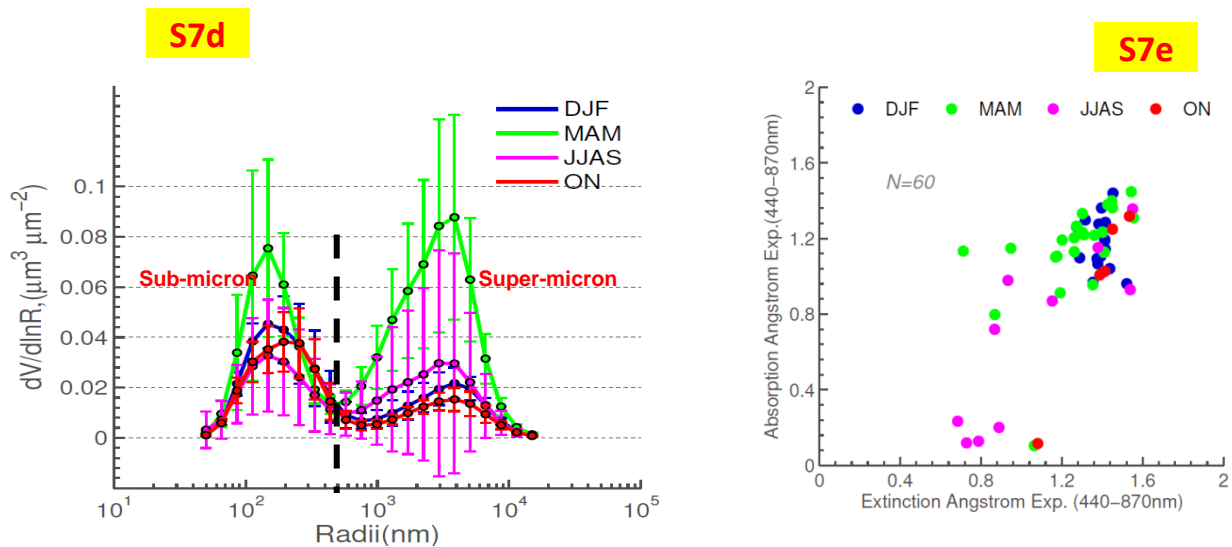


Figure S7. The AERONET-based aerosol optical depth and radiative properties in the Pokhara Valley from 2010 to 2016. Monthly summaries are presented using level 2 collections and supplemented with level 1.5 for missing data points; (**S7a**) AOD at seven wavelengths; (**S7b**) Inversion products such as fine AOD (AOD-F), coarse AOD (AOD-C), and total AOD (AOD-T), along with Ångstrom exponent (440-870 nm, magenta line); (**S7c**) AOD-T for Kanpur, Gandi Nagar (both IGP sites in India) and the NCO-P site (labeled EVK2-CNR, a high altitude site in the Khumbu Valley at the base of Mt. Everest); (**S7d**) Seasonal average of volume particle size distribution grouped by four seasons (the error bar indicates the standard deviation, and the uncertainty in the calculated size distribution is close to 20 % in the range $0.2 \mu\text{m} < D_p < 14 \mu\text{m}$). The four seasons are classified as winter (DJF: December, January and February), monsoon (JJAS: June, July, August and September), pre-monsoon (MAM: March, April and May) and post-monsoon (ON: October and November); (**S7e**) absorption Ångstrom exponent (440-870) and extinction Ångstrom exponent (440-870 nm), color-coded for the four seasons

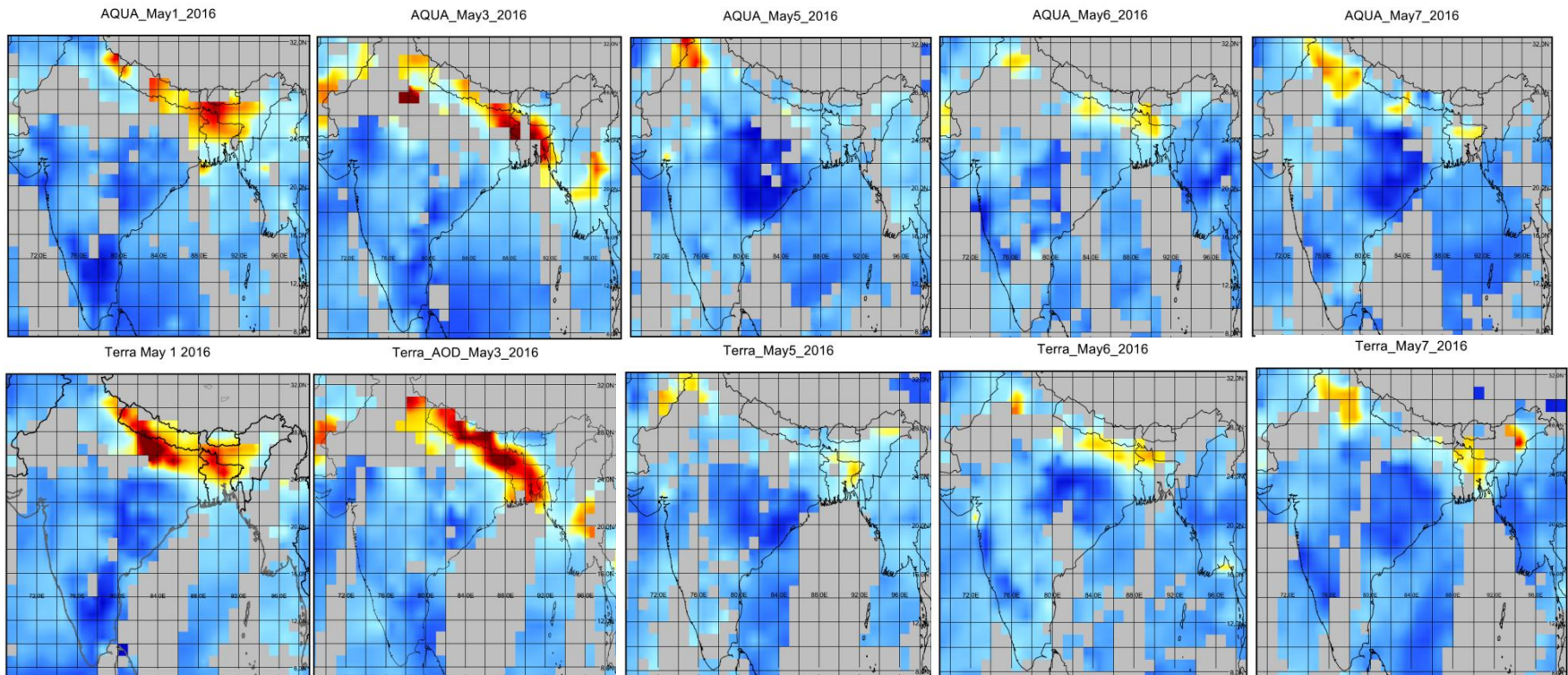


Figure S8: MODIA AQUA AND TERRA AOD at 550 nm over the IGP and Himalayan region from 1 – 7 May. The plots were generated using the Level-3 MODIS Atmosphere Daily products, ***MOD08_D3*** at ($1^{\circ} \times 1^{\circ}$) resolution. Top panel (AQUA) and bottom panel (TERRA).

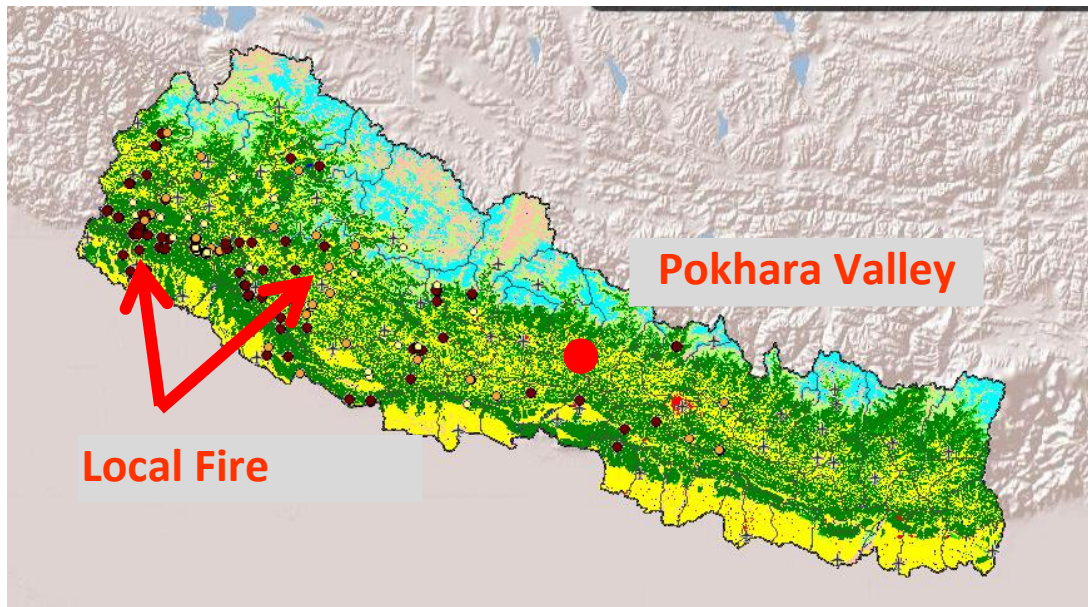


Figure S9: Locally or nationally recorded active fire for the same period by the National Emergency Operation Centre (<http://neoc.gov.np/en/>) via the ICIMOD portal (<http://118.91.160.238/NepalForestFire/index.html>)

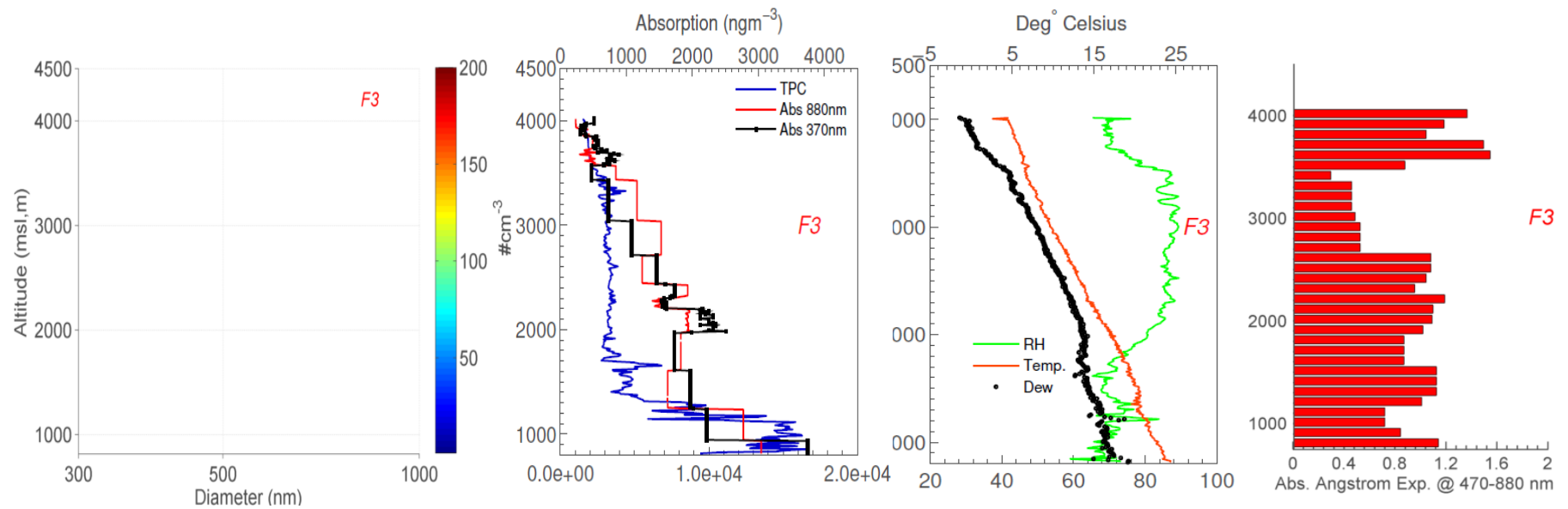


Figure S10: Morning test flight (Flight F3) on 6 May 2016 is shown here, the rest of the results are already shown in in Figure. Each subplot is arranged by (i) Aerosol number size distribution measured by the Grimm OPC model 1.108 (0.3-20 μm), limited to 1 μm in the figure, (ii) Total particle number concentration (also indicated as **TPC**, $D_p > 11 \text{ nm}$) measured by the TSI CPC 3760 and absorption aerosol at 370 nm and 880 nm (iii) temperature ($^{\circ}\text{C}$) and dew point (black dot, in $^{\circ}\text{C}$) and relative humidity (or RH %), (iv) calculated absorption Ångstrom exponent averaged for every 100 meters elevation band.

Figure S11: Estimating the AAE value using the power fit and linear fit (left: power fit, right: linear fit)

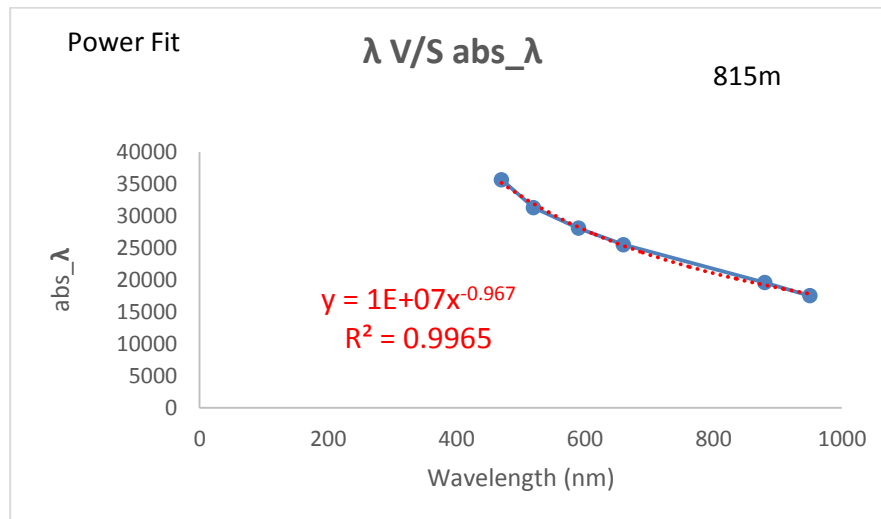
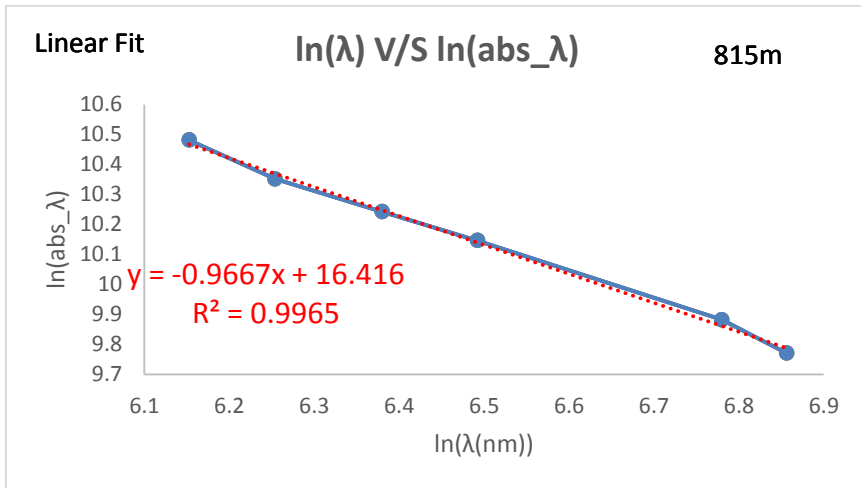


Table S1

Flight #	Flight date	Flight time window		Measured parameter
F1	5 May 2016	7:00-9:00	Morning flight	T,RH, total particle count, number-size distribution, BC
F2	5 May 2016	14:00-17 :00	Afternoon flight	"
F3	6 May 2016	7:00-9:00	Morning flight	"
F4	6 May 2016	14:00-17 :00	Afternoon flight	"
F5	7 May 2016	7:00-9:00	Morning flight	"